Chinese Chemical Letters 36 (2025) 109939

Contents lists available at ScienceDirect

Chinese Chemical Letters

journal homepage: www.elsevier.com/locate/cclet

Highly selective QCM sensor based on functionalized hierarchical hollow TiO_2 nanospheres for detecting ppb-level 3-hydroxy-2-butanone biomarker at room temperature

Siqi Sun[a,1], Cheng Zhao[a,b,1], Zhaohuan Zhang[a], Ding Wang[c], Xinru Yin[a], Jingting Han[a], Jinlei Wei[a], Yong Zhao[a,*], Yongheng Zhu[a,*]

[a] College of Food Science and Technology, Laboratory of Quality & Safety Risk Assessment for Aquatic Products on Storage and Preservation (Shanghai), Ministry of Agriculture and Shanghai Engineering Research Center of Aquatic Product Processing & Preservation, Shanghai Ocean University, Shanghai 201306, China

[b] Henan Railway Food Safety Management Engineering Technology Research Center, Zhengzhou Railway Vocational & Technical College, Zhengzhou 451460, China

[c] School of Materials Science and Engineering, University of Shanghai for Science and Technology, Shanghai 200093, China

ARTICLE INFO

Article history:
Received 30 January 2024
Revised 11 March 2024
Accepted 28 April 2024
Available online 29 April 2024

Keywords:
Hierarchical hollow TiO_2 nanospheres
AAPTMS functionalization
Gas sensor
3-Hydroxy-2-butanone detection
Sensing mechanism

ABSTRACT

Listeria monocytogenes (*LM*) is a dangerous foodborne pathogen for humans. One emerging and validated method of indirectly assessing *LM* in food is detecting 3-hydroxy-2-butanone (3H2B) gas. In this study, the synthesis of 3-(2-aminoethylamino) propyltrimethoxysilane (AAPTMS) functionalized hierarchical hollow TiO_2 nanospheres was achieved *via* precise controlling of solvothermal reaction temperature and post-grafting route. The sensors based on as-prepared materials exhibited excellent sensitivity (480 Hz@50 ppm), low detection limit (100 ppb), and outstanding selectivity. Moreover, the evaluation of *LM* with high sensitivity and specificity was achieved using the sensors. Such stable three-dimensional spheres, whose distinctive hierarchical and hollow nanostructure simultaneously improved both sensitivity and response/recovery speed dramatically, were spontaneously assembled by nanosheets. Meanwhile, the moderate loadings of AAPTMS significantly improved the selectivity of sensors. Then, the gas-sensing mechanism was explored by utilizing thermodynamic investigation, Gaussian 16 software, and *in situ* diffuse reflectance infrared transform spectroscopy, illustrating the weak chemisorption between the -NH- group and 3H2B molecules. These portable sensors are promising for real-time assessment of *LM* at room temperature, which will make a magnificent contribution to food safety.

Listeriosis, caused by the bacterium *Listeria monocytogenes* (*LM*), is a highly severe foodborne illness worldwide [1]. Its clinical encompass diarrhea, septicemia, miscarriage, and meningitis [2], with a fatality rate typically ranging from 20%–30% [3]. Currently, the most commonly used method regarding the detection of *LM* is still the traditional and less efficient culture-based identification method. Diagnostic techniques based on molecular biology [4], and immunology offer faster response time [5]. However, they may occasionally yield false positive results or be susceptible to interference from matrix backgrounds [6]. Therefore, it is of utmost practical significance to establish a rapid, convenient, ultrasensitive, and highly selective detection method for controlling *LM* infection and contamination.

Microorganisms are known to generate microbial volatile organic compounds (MVOCs) during metabolism that are considered to be biomarkers [7]. When *LM* multiplies in foods, it produces a large amount of exhaled gas, in which 3-hydroxy-2-butanone (3H2B) is the characteristic biomarker with an abundance of more than 32.18% [8,9]. Nowadays, there has been a growing interest in methods to indirectly assess microbial contamination by detecting MVOCs in real time through noninvasive and rapid operations. Cheng *et al.* used E-nose and GC–MS to identify flavor substances, such as 3H2B, in Tibetan pork from different cooking methods [10]. Tian *et al.* prepared urchin-like mesoporous WO_3 and identified 3H2B at 240 °C [11]. However, the disadvantages of these methods are expensive to operate, require highly skilled analysts and time-consuming techniques, which cannot be used for real-time moni-

* Corresponding authors.
E-mail addresses: yzhao@shou.edu.cn (Y. Zhao), yh-zhu@shou.edu.cn (Y. Zhu).
[1] These authors contributed equally to this work.

https://doi.org/10.1016/j.cclet.2024.109939
1001-8417/

toring of 3H2B at room temperature. In this regard, the advantages of the quartz crystal microbalance (QCM), such as low power consumption, miniaturization, cost-effectiveness [12,13], and high sensitivity [14], make it capable of effectively detecting 3H2B [15].

Since the bare QCM electrode's weak response to target gas molecules, modifying sensitive materials on the electrode can improve the gas sensing performance. In previous studies, various sensitive materials have been explored, including semiconductor metal oxides, polymer, and mesoporous carbon [16-18]. As a type of semiconductor metal oxide, titanium dioxide (TiO_2) has favorable chemical stability and is suitable for sensing layers [19-21]. Nevertheless, the selectivity and sensitivity of most pristine TiO_2 gas sensors are still not very satisfactory. To address the limited response capability of gas sensing materials especially pristine TiO_2 towards target gases, morphological control and structural modification of the sensitive materials is a very effective strategy [22-25]. Until now, hierarchical and hollow oxide nanostructures have been very reliable gas sensor materials because of their high surface area and well-aligned nanoporous structures. Specifically, owing to the greater dimensions and high dispersion, three-dimensional hierarchical structures are relatively robust, therefore enhancing the stability of gas sensing [26]. Meanwhile, the hollow nanostructure can enhance gas sensing performance *via* increasing the number of active sites available for gas adsorption and improving the target gas diffusion process [27]. Besides, surface functionalization of gas-sensitive materials also profits to effectively enhance the selectivity of gas sensors. For instance, Chen *et al.* noticed that the hydrophobic Cu(I)-Cys nanocomposite based QCM sensor exhibits good sensitivity and selectivity to hexanal and 1-octen-3-ol [28]. Cao *et al.* designed urea-functionalized SBA-15 for dimethyl methylphosphonate detection with rapid response and high selectivity [29]. According to previous research, 3-(2-aminoethylamino) propyltrimethoxysilane (AAPTMS) can conveniently and effectively functionalize sensing materials by providing active amino groups, which is believed to have unique weak chemisorption with 3H2B molecules [30]. Thus, the study of hierarchical hollow nanomaterials with amine functionalization holds significant importance in enabling real-time analysis of trace 3H2B levels at room temperature.

In this paper, a simple synthesis was reported that the hierarchical hollow TiO_2 nanospheres (HHS-TiO_2-200) were self-organized from ultrathin anatase TiO_2 nanosheets. Subsequently, AAPTMS was modified onto the surface of nanospheres by the post-grafting method. Finally, the QCM gas sensor was constructed based on these sensing materials (Scheme 1). To verify the optimal loadings of AAPTMS, the sensing performance of pristine HHS-TiO_2-200 and different amino loadings of HHS-TiO_2-200 (NH_2-1@HHS-TiO_2-200, NH_2-2@HHS-TiO_2-200, and NH_2-3@HHS-TiO_2-200) were investigated. Among them, NH_2-2@HHS-TiO_2-200 has the most desirable properties for detecting 3H2B, because appropriate amino loadings significantly enhanced the sensitivity (480 Hz@50 ppm) and selectivity of the sensors towards 3H2B, and reduced the response/recovery time (6/7 s@50 ppm). These remarkable gas-sensing properties are ascribed to weak chemisorption occurring between the –NH– functional group of AAPTMS and 3H2B molecules.

The controllable construction of uniformly dispersed TiO_2 nanospheres with different morphologies was achieved *via* tuning the reaction temperature. Morphology and structural characteristics of all pristine TiO_2 nanospheres (Fig. S1 in Supporting information) were investigated by SEM. When the heating temperature was 160 °C, spherical particles with a diameter of approximately 38 nm piled up into TiO_2-160 nanospheres (Figs. S1a-c). With the increase of heating temperature (200 °C), the pellets gradually stretched and thinned, forming layered ultrathin anatase HHS-TiO_2-200 without any signs of aggregation (Figs. S1d-f). HHS-

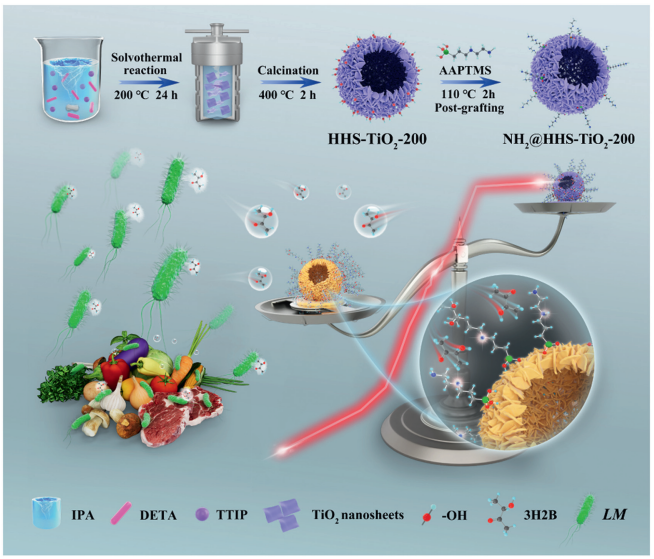

Scheme 1. Diagrammatic sketch of the synthesis and application process of NH_2@HHS-TiO_2-200.

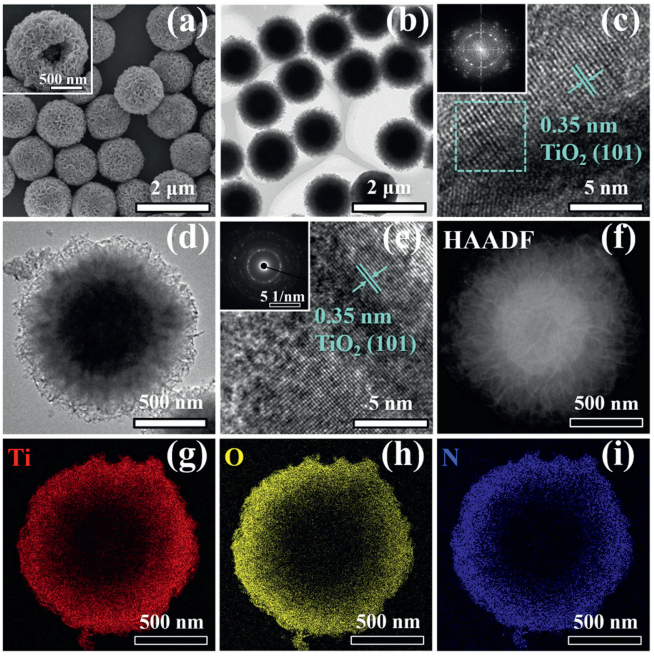

Fig. 1. (a) SEM (in which the inset showed the hollow structure of a cracked sphere), (b) TEM and (c) HRTEM images (in which the inset showed FFT-ED graphics of the marked zone) of HHS-TiO_2-200. (d) TEM, (e) HRTEM and SAED images of NH_2-2@HHS-TiO_2-200. (f–i) STEM-EDS elemental mapping images of NH_2-2@HHS-TiO_2-200.

TiO_2-200 showed a hollow structure, as indicated by the presence of cracked nanospheres (Fig. S1d and the insert in Fig. 1a), resulting in a large specific surface area and excellent gas-sensing performance (details described below). It was revealed that the constituent nanosheets were clearly visible and exhibited random orientations, as observed in Figs. 1a and b. Fig. 1c presented a piece of single nanosheet with visible lattice fringe spacings of 0.35 nm, corresponding to the anatase (101) plane of TiO_2 [31]. The TEM analysis results were confirmed by the fast Fourier transform electron diffraction (FFT-ED) graphic of the same region (the inset of Fig. 1c), which represented good crystallinity of HHS-TiO_2-200. Besides, compared with TiO_2-160 in Figs. S1a-c, the diameter of

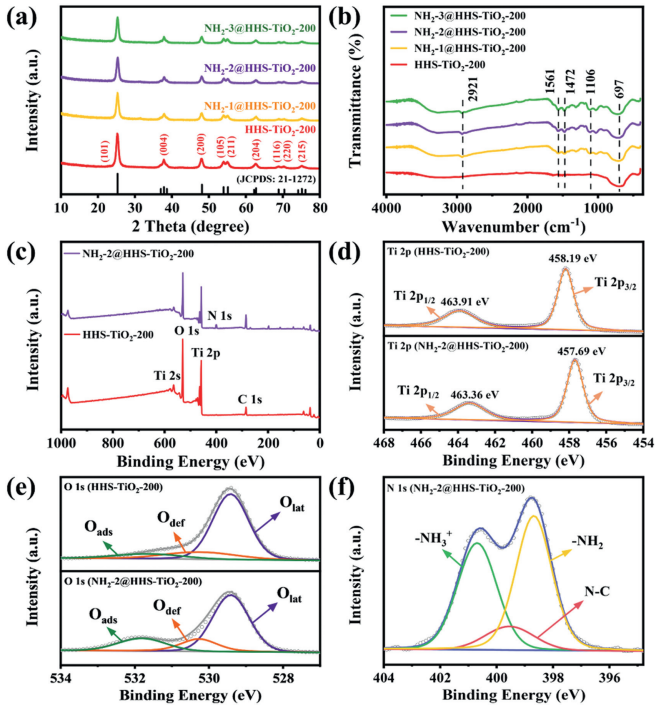

Fig. 2. (a) XRD patterns, (b) FT-IR spectra of HHS-TiO_2-200, NH_2-1@HHS-TiO_2-200, NH_2-2@HHS-TiO_2-200, and NH_2-3@HHS-TiO_2-200. (c) XPS full spectrum of HHS-TiO_2-200, NH_2-2@HHS- TiO_2-200. High-resolution XPS spectrums of (d) Ti 2p and (e) O 1s of HHS-TiO_2-200 and NH_2-2@HHS-TiO_2-200, and (f) N 1s of NH_2-2@HHS-TiO_2-200.

HHS-TiO_2-200 in Figs. S1d-f was increased to 1.4 μm, and the thickness of nanosheets was about 22 nm. After further increasing the heating temperature to 240 °C, the interior of TiO_2-240 consisted of cross-homogeneous nanorods, whose width was at 28 nm, with reducing nanospheres particle size to 600 nm (Figs. S1g-i).

The specific morphology, structural and composition characterizations NH_2-2@HHS-TiO_2-200 were shown in Figs. 1d-i. As exhibited in Figs. 1d and e, the three-dimensional hierarchical spherical structure and the maintenance of lattice fringe spacings were observed from NH_2-2@HHS-TiO_2-200. Obviously, the samples after amine functionalization treatment still had high stability. The selected area electron diffraction (SAED) pattern (the inset in Fig. 1e) of NH_2-2@HHS-TiO_2-200 verified the polycrystalline nature of the sample. Each diffraction ring easily pointed to anatase TiO_2, confirming the XRD results [32]. The elemental mapping images of NH_2-2@HHS-TiO_2-200 were depicted in Figs. 1f-i. Evidently, AAPTMS were uniformly dispersed on the surface of TiO_2 nanospheres.

The crystalline phase structures and the purity of the pristine TiO_2 nanospheres and NH_2@HHS-TiO_2-200 were investigated by XRD. All detected diffraction peaks were precisely consistent with anatase TiO_2 (JCPDS No. 21-1272), as presented in Fig. 2a and Fig. S2 (Supporting information) [33]. No other impurity peaks were observed, confirming the high purity of all TiO_2 products. Following the amine functionalization procedure, there was no shift in the peak positions of NH_2@HHS-TiO_2-200, suggesting a high degree of material stability. However, the diffraction peak intensity was slightly reduced owing to the doping of AAPTMS, indicating a reduction in the crystallinity of the mesoporous material rather than a collapse of the pore structure [34].

FT-IR spectroscopy was utilized to investigate the presence of amine functional groups on NH_2@HHS-TiO_2-200. Fig. 2b displayed the FT-IR spectrum of as-prepared samples. At low frequencies, a descending band was determined in all samples in the range of 512–878 cm^{-1}, matching the Ti–O–Ti bond [35], indicating the formation of TiO_2. All the spectra of NH_2-1@HHS-TiO_2-200, NH_2-2@HHS-TiO_2-200 and NH_2-3@HHS-TiO_2-200 had peaks around 1106 cm^{-1}, corresponding to the stretching vibrations of Si–O–Si groups [36]. The organosilane's C–H stretching produced peaks that ranged from 2888 cm^{-1} to 2970 cm^{-1}. Besides, there were peaks at 1561 and 1472 cm^{-1}, which corresponded to stretching and deformation frequencies of –NH– and $-NH_3^+$, respectively. It was demonstrated that the amine-functionalized material has been successfully obtained [34].

XPS was performed to further examine the valence states and chemical composition of HHS-TiO_2-200 and NH_2-2@HHS-TiO_2-200. The full survey spectrum (Fig. 2c) showed that all samples contained Ti, O, and C elements. Furthermore, a peak at 399.08 eV was assigned to the binding energy of N 1s, verifying the existence of amino groups. As shown in Fig. 2d, the peaks of Ti $2p_{1/2}$ (463.91 and 463.36 eV) and Ti $2p_{3/2}$ (458.19 and 457.69 eV) indicated that the Ti element was almost unaffected by AAPTMS doping [37]. The O 1s peaks at 531.79, 530.29, and 529.42 eV belonged to adsorbed oxygen (O_{ads}), defect oxygen (O_{def}), and lattice oxygen (O_{lat}), respectively (Fig. 2e). In HHS-TiO_2-200, the proportion of O_{ads} and O_{def} were 10.3% and 15.5%, respectively. After being decorated by AAPTMS, their proportions increased to 18.7% and 16.1%. This facilitated the surface adsorption and catalytic conversion of target gas [38]. The N 1s spectra was decoupled into three peaks in Fig. 2f. The N–C bond and $-NH_2$ were characterized by the peaks at 398.7 and 399.5 eV, respectively. Meanwhile, the peak at 400.7 eV was assigned to the interaction between the proton and the amidogen ($-NH_3^+$) [39].

N_2 adsorption-desorption isotherms of samples and the gas sensing properties of QCM sensors based on the pristine TiO_2 nanospheres were described in detail in Figs. S3 and S4 (Supporting information), respectively. These results further confirmed that HHS-TiO_2-200 was the optimal TiO_2 material for amine functionalization. Then, the gas sensing properties of HHS-TiO_2-200, NH_2@HHS-TiO_2-200-based sensors were investigated. As shown in Fig. 3a, upon the introduction of 3H2B, all the sensors represented rapid response and returned promptly to their initial state in ambient air. The response of QCM gas sensors is defined as the value of frequency shift, whose unit is Hz. Notably, the NH_2-2@HHS-TiO_2-200-based QCM sensor displayed the largest response across all concentrations, indicating that the most optimal AAPTMS loading amounts were 2.06 mmol/g. The response values exhibited an increase or decrease following the concentration of 3H2B, thereby revealing the excellent repeatability and reversibility of these sensors. In addition, as depicted in Fig. 3b, a favorable linear relationship was observed between the response values of each sensor and various concentrations of 3H2B. This characteristic facilitated the quantitative measurement of 3H2B in practical utilizations.

The response/recovery speed of the sensors, which is defined as the time taken to reach 90% equilibrium from the beginning condition, is a crucial parameter for evaluating its real monitoring ability of target gases [40]. The response/recovery time of HHS-TiO_2-200 and NH_2-2@HHS-TiO_2-200 sensors were 9/11 s and 6/7 s, respectively, when exposed to 50 ppm 3H2B (Fig. 3c). The excellent response time of the NH_2-2@HHS-TiO_2-200 sensor stemmed from the following factors. Firstly, the high specific surface area of HHS-TiO_2-200 made gas molecules adsorption easier. Then, -NH- groups in AAPTMS underwent weak chemisorption with 3H2B molecules forming chemical bonds, which improved the gas selectivity.

The identification of target gases in complex physical environments is crucial for gas sensors. Therefore, the selectivity of NH_2-2@HHS-TiO_2-200-based sensors was investigated to assess its resistance against interference. To evaluate the selectivity of NH_2-2@HHS-TiO_2-200-based sensors, their responses to various gases (50 ppm) were measured, including acetic acid, acetophe-

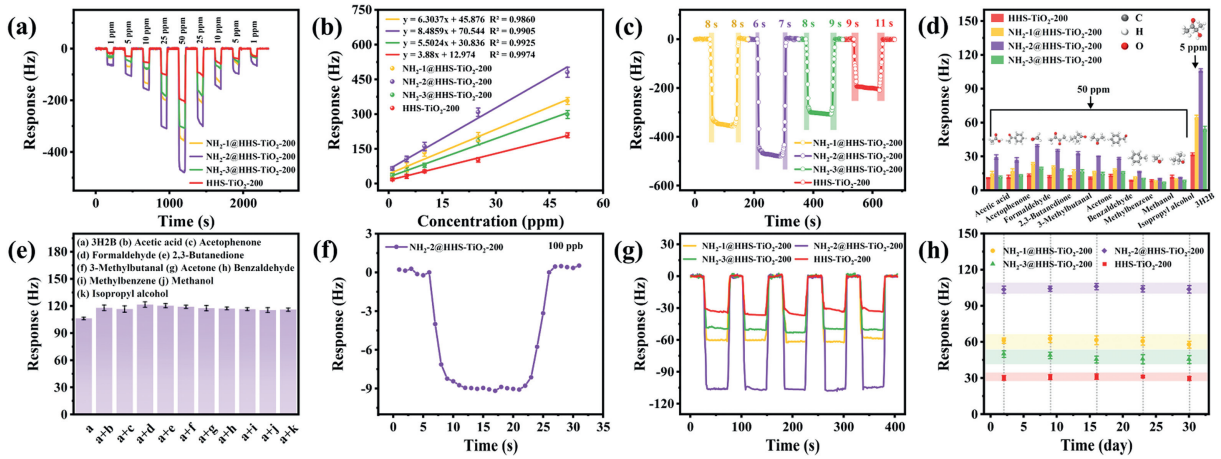

Fig. 3. Gas-sensing properties of the HHS-TiO_2-200 and NH_2@HHS-TiO_2-200-based sensors towards varying levels of AAPTMS loadings: (a) Dynamic responses to 3H2B (1–50 ppm); (b) Relationship between responses and 3H2B concentration (1–50 ppm); (c) Response/recovery time of the sensors to 3H2B (50 ppm); (d) Selectivity of the HHS-TiO_2-200, NH_2@HHS-TiO_2-200-based sensors (5 ppm 3H2B and 50 ppm other interfering gases); (e) Discrimination test of NH_2-2@HHS-TiO_2-200 sensors to the mixed gases containing 5 ppm 3H2B and 50 ppm other interfering gases; (f) Response of NH_2-2@HHS-TiO_2-200 to 3H2B (100 ppb); (g) Repeatability and (h) long-term stability of the HHS-TiO_2-200, NH_2@HHS-TiO_2-200-based sensors to 3H2B (5 ppm).

none, formaldehyde, 3-methylbutanal, acetone, methylbenzene, methanol, and isopropyl alcohol. The NH_2-2@HHS-TiO_2-200-based sensors exhibited excellent selectivity towards 5 ppm 3H2B with minimal interference from other gases (Fig. 3d). Notably, two common exhaled gases of *LM*: 2,3-butanonedione (abundance of MVOCs: 11.55%) and benzaldehyde (abundance of MVOCs: 17.16%) were chosen as interfering gases, because they were the most prevalent MVOCs of *LM*, after 3H2B [8]. Even at a concentration of 50 ppm, the response of NH_2-2@HHS-TiO_2-200-based sensors to 3H2B was at least three times larger than that towards the two tested interfering gases. It was demonstrated that NH_2@HHS-TiO_2-200-based QCM sensors obtained magnificent selectivity towards 3H2B emitted by *LM*. Additionally, the discriminant test results of NH_2-2@HHS-TiO_2-200-based sensors were illustrated in Fig. 3e. The responses varied within a 15% range when mixtures containing 5 ppm 3H2B and 50 ppm various interfering gases were analyzed. These results undoubtedly demonstrated the excellent selectivity of NH_2-2@HHS-TiO_2-200-based sensors. Simultaneously, as shown in Fig. S5 (Supporting information), the frequency shifts of prepared gas sensors towards 5 ppm 3H2B changed slightly with increasing relative humidity. It was indicated that the impact of water vapor on NH_2-2@HHS-TiO_2-200-based sensor was less than 3H2B, which possessed a higher molecular weight than water molecules and exerted a stronger positive induction effect [41]. In addition, the NH_2-2@HHS-TiO_2-200-based sensor had a quite low detection limit, which was 9 Hz even for 3H2B at 100 ppb (Fig. 3f).

Repeatability is also a crucial indicator of gas sensors. Sensors based on HHS-TiO_2-200, NH_2-1@HHS-TiO_2-200, NH_2-2@HHS-TiO_2-200, and NH_2-3@HHS-TiO_2-200 remained constant for five cycles to 5 ppm 3H2B. The response-recovery curves of all sensors reappeared with small changes, as depicted in Fig. 3g, indicating their excellent repeatability. Similarly, Fig. S6 (Supporting information) demonstrated that the repeatability of NH_2-2@HHS-TiO_2-200-based sensor towards 100 ppb 3H2B remained quite good, which further confirmed the low detection limit of the sensor. Additionally, Fig. 3h revealed that the long-term stability of the sensors was evidenced by the negligible change in response values. Table S1 (Supporting information) compared the gas-sensing performance of various sensors towards gases, whose molecules contain carbonyl in this study and previous studies. It was illustrated that NH_2-2@HHS-TiO_2-200-based sensors represented exceptional sensitivity (160.70 Hz), rapid response/recovery time (4/7 s), and low power consumption, highlighting its potential for practical applications of swiftly detecting 3H2B.

By assessing the gas produced during the proliferation of *LM* in BHI broth, the practical application potential of NH_2-2@HHS-TiO_2-200-based sensors has been further evaluated. The response of these sensors varied inconspicuously at beginning and then significantly as culture time passed, which coincident with the shift in OD values (Figs. S7a and b in Supporting information). Countries that are members of the European Union stipulate that food should have an *LM* concentration of no more than 10^2 CFU/g [42]. The visible response to *LM* with an original concentration of 10 CFU/mL was observed after 14 h of proliferation, and the frequency shift came to 18.67 Hz after 18 h of incubation (Fig. S7b). The results indicated that the sensors could completely comply with food safety standards. Furthermore, two kinds of typical foodborne pathogen, *Staphylococcus aureus* and *Escherichia coli*, were evaluated as well. It was demonstrated that the response towards *LM* (10^3 CFU/mL) was significantly higher than the response to *Staphylococcus aureus* (10^6 CFU/mL) and *E. coli* (10^6 CFU/mL), which proved the satisfactory selectivity of the sensor (Fig. S7c in Supporting information). Thus, all the above results confirmed the feasibility of detecting *LM* with high sensitivity and excellent selectivity *via* NH_2-2@HHS-TiO_2-200 sensors.

The basis for a QCM gas sensor is mass sensitivity [43]. In principle, intermolecular forces promote the adsorption process of gas molecules onto the surface of the mass-sensitive chemical sensors. These forces originate from typical hydrogen bonding and van der Waals interactions, which enable the accumulation of gas molecules on solid sensitive materials. The adsorption and desorption properties of NH_2-2@HHS-TiO_2-200, HHS-TiO_2-200 and TiO_2-160 materials for 3H2B were displayed in Fig. 4a. NH_2-2@HHS-TiO_2-200 had superior gas-sensing performance compared to HHS-TiO_2-200 and TiO_2-160. The high response and rapid response kinetics of the gas were attributed to the better permeability of the hollow structure, which favored the fast and efficient diffusion of 3H2B molecules across the entire TiO_2 materials. Moreover, the surface functional groups and defect sites of sensitive materials are the main factors that affect the gas adsorption capacity. Numerous active sites were obtained by the designed HHS-TiO_2-200, increasing the amount of 3H2B molecules that can be absorbed. Meanwhile, the increase in active sites provided more AAPTMS attachment scaffolds. The amino group in AAPTMS can react reversible Schiff base with 3H2B molecules, thereby effectively improving the

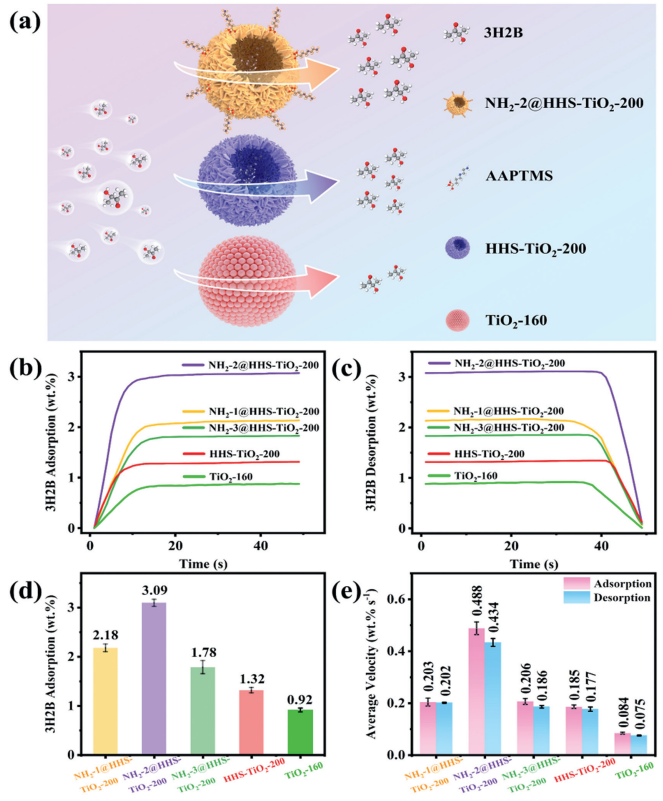

Fig. 4. (a) Schematic diagram of 3H2B adsorption and desorption processes of NH_2-2@HHS-TiO_2-200, HHS-TiO_2-200 and TiO_2-160. (b–e) 3H2B adsorption performance test of QCM gas sensors based on NH_2-1@HHS-TiO_2-200, NH_2-2@HHS-TiO_2-200, NH_2-3@HHS-TiO_2-200, HHS-TiO_2-200, and TiO_2-160.

chemical selectivity of the sensor [44]. Thus, the presence of –NH– functional groups in the hierarchical structure resulted in highly specific sensing properties. The effect of different AAPTMS loadings on HHS-TiO_2-200 was further investigated through isothermal adsorption/desorption measurements conducted on NH_2-1@HHS-TiO_2-200, NH_2-2@HHS-TiO_2-200, NH_2-3@HHS-TiO_2-200, HHS-TiO_2-200 and TiO_2-160. The adsorption and desorption curves of 3H2B were depicted in Figs. 4b and c, respectively. The addition of AAPTMS in appropriate amounts enhanced both the adsorption and desorption capacities of the material surface [45]. Hence, the efficient adsorption of the amino group to 3H2B was fully optimized by NH_2-2@HHS-TiO_2-200, showing the largest adsorption capacity (3.09 wt%) and the quickest average adsorption rate (0.488 wt%/s) for 3H2B (Figs. 4d and e). In addition, thermodynamic investigation (Fig. S8 in Supporting information), Gaussian calculation (Fig. S9 in Supporting information), and *in situ* diffuse reflectance infrared transform spectroscopy (DRIFTS) analysis (Fig. S10 in Supporting information) were carried out, further verifying the weak chemisorption between the -NH- group and 3H2B molecules (details were described in Supporting information).

In summary, TiO_2 microspheres with different nanostructures were smoothly prepared using a simple solvothermal method with reasonably adjusted reaction temperature appropriately. The uniform HHS-TiO_2-200, which was self-assembled from ultrathin anatase TiO_2 nanosheets obtained at 200 °C with a quite high specific surface area (139.96 m^2/g), had the best gas sensing performance among pristine TiO_2 nanospheres. After amine functionalization, NH_2-2@HHS-TiO_2-200-based sensors revealed outstanding response (480 Hz@50 ppm) to 3H2B with high selectivity, fast response/recovery time (6/7 s@50 ppm) and good stability. Especially, the constructed sensor could generate response towards ppb-levels 3H2B (100 ppb). Then, NH_2-2@HHS-TiO_2-200-based sensors were utilized to detect *LM* incubated in BHI culture medium with high sensitivity and specificity. In addition, the thermodynamic investigation, Gaussian simulations and *in situ* DRIFTS results proved that a reversible weak chemisorption played an important role between NH_2-2@HHS-TiO_2-200 and 3H2B molecules. This study provides a facile synthesis method, rational nanostructure design, and comprehensive mechanism exploration for the application of TiO_2-based QCM sensors in real-time and nondestructive detection of *LM*.

Declaration of competing interest

The authors declare that they have no known competing financial interests or personal relationships that could have appeared to influence the work reported in this paper.

Acknowledgments

This work was financially supported by the National Natural Science Foundation of China (No. 32272399), and the Shanghai Natural Science Foundation (No. 21ZR1427500).

Supplementary materials

Supplementary material associated with this article can be found, in the online version, at doi:10.1016/j.cclet.2024.109939.

References

[1] C. Fang, X.Y. Chen, X.Y. Liang, et al., Kafkas Univ. Vet. Fak. Derg. 25 (2019) 665–672.
[2] L.H. Kuang, Y.Y. Lai, Y.H. Gong, J. Obstet. Gynaecol. Res. 48 (2022) 66–72.
[3] S. Liu, X.L. He, T. Zhang, et al., Chin. Chem. Lett. 33 (2022) 1933–1935.
[4] D.K. Soni, R. Ahmad, S.K. Dubey, Crit. Rev. Microbiol. 44 (2018) 590–608.
[5] D. Wang, Q. Chen, H.L. Huo, et al., Food Control 73 (2017) 555–561.
[6] L. Wang, P.P. Zhao, X.X. Si, et al., Front. Microbiol. 10 (2020) 2959.
[7] Y. Wang, Y.X. Li, J.L. Yang, J. Ruan, C.J. Sun, Trends Anal. Chem. 78 (2016) 1–16.
[8] Y.X. Yu, X.H. Sun, Y. Liu, Y.J. Pan, Y. Zhao, Can. J. Microbiol. 61 (2015) 367–372.
[9] Y.H. Zhu, Y. Zhao, J.H. Ma, et al., J. Am. Chem. Soc. 139 (2017) 10365–10373.
[10] L.J. Cheng, X. Li, Y.T. Tian, et al., Food Chem. X 19 (2023) 100873.
[11] Y.C. Tian, D.P. Xu, C. Liu, et al., Mater. Sci. Semicond. Process 137 (2022) 106160.
[12] X.T. Fang, L.Y. Wang, X. He, J.Q. Xu, Z.M. Duan, Inorg. Chem. 57 (2018) 1689–1692.
[13] J.S. Malhotra, M. Kubus, K.S. Pedersen, S.I. Andersen, J. Sundberg, ACS Sens. 8 (2023) 3478–3486.
[14] S. Chen, X. Duan, C. Liu, et al., J. Hazard. Mater. 467 (2024) 133672.
[15] J. Zong, Y.S. Zhang, Y. Zhu, et al., Sens. Actuator. B: Chem. 271 (2018) 311–320.
[16] F. Li, X. Gao, R. Wang, T. Zhang, G.Y. Lu, Sens. Actuator. B: Chem. 248 (2017) 812–819.
[17] Y. Chen, L.Y. Wang, J.W. Kong, B. Shen, J.Q. Xu, Chin. Chem. Lett. 31 (2020) 2125–2128.
[18] J.J. Qiu, D.M. Ke, H.C. Lin, et al., Chin. Chem. Lett. 34 (2023) 107391.
[19] L. Mardiana, A.Y.P. Wardoyo, H.A.Dharmawan Masruroh, Pol. J. Environ. Stud. 32 (2023) 1735–1742.
[20] T. Zhao, P.P. Qiu, Y. Fan, et al., Adv. Sci. 6 (2019) 1902008.
[21] Y. Liu, Y.F. Luo, A.A. Elzatahry, et al., ACS Central Sci. 1 (2015) 400–408.
[22] W.H. Yan, W.R. Yan, T.D. Chen, et al., ACS Appl. Nano Mater. 3 (2020) 2545–2553.
[23] H.F. Zhang, J.Y. Xuan, Q. Zhang, et al., Rare Metals 41 (2022) 3976–3999.
[24] X.W. Cheng, L. Huang, X.Y. Yang, et al., J. Colloid Interface Sci. 535 (2019) 425–435.
[25] Y. Liu, Z.R. Wang, W. Teng, et al., J. Mater. Chem. A 6 (2018) 3162–3170.
[26] Y. Yang, Y. Liang, G.Z. Wang, et al., ACS Appl. Mater. Interfaces 7 (2015) 24902–24908.
[27] Y.G. Wang, L.C. Yao, L.J. Xu, et al., Mater. Lett. 302 (2021) 130460.
[28] W. Chen, Z.H. Wang, S. Gu, et al., Sens. Actuator. B: Chem. 305 (2020) 127476.
[29] Y.S. Cao, Y. Fan, Z.H. Ma, et al., Sens. Actuator. B: Chem. 273 (2018) 1162–1169.
[30] S. Karapati, T. Giannakopoulou, N. Todorova, et al., Appl. Catal. B: Environ. 176 (2015) 578–585.
[31] F.Y. Song, H. Sun, H.L. Ma, H. Gao, Nanomaterials 12 (2022) 2536.
[32] G.Q. Zhang, H.B. Wu, T. Song, U. Paik, X.W. Lou, Angew. Chem. Int. Ed. 53 (2014) 12590–12593.
[33] A. Alshehri, K. Narasimharao, J. Mater. Res. Technol. 9 (2020) 14907–14921.
[34] Y.H. Zhu, H. Li, Q. Zheng, J.Q. Xu, X.X. Li, Langmuir 28 (2012) 7843–7850.

[35] A.R. Jimenez, D. Nuñez, N. Rojas, Y. Ramirez, M. Acevedo, ACS Omega 6 (2021) 4932–4938.
[36] X. Zhao, P. Dai, D.Y. Xu, et al., J. Energy Chem. 59 (2021) 455–464.
[37] L. Ren, W. Zhu, Y.H. Li, et al., Nano-Micro Lett. 14 (2022) 144.
[38] K.Y. Chen, W.H. Xie, Y. Deng, et al., ACS Nano 17 (2023) 15763–15775.
[39] X. Fang, S.B. Wu, Y.H. Wu, et al., Appl. Surf. Sci. 518 (2020) 146226.
[40] Z.Y. Zhu, L.J. Zheng, S.Z. Zheng, et al., J. Mater. Chem. A 6 (2018) 21419–21427.
[41] W. Chen, F.F. Deng, M. Xu, et al., Sens. Actuator. B: Chem. 273 (2018) 498–504.
[42] S.Q. Xie, C. Zhao, J.B. Shen, et al., ACS Sens. 8 (2023) 728–738.
[43] Y.H. Zhu, X.H. Dong, J.S. Cheng, et al., Chin. Chem. Lett. 34 (2023) 107930.
[44] L.Y. Wang, Z.X. Wang, Q. Xiang, et al., Sens. Actuator. B: Chem. 248 (2017) 820–828.
[45] H.J. Cai, N. Luo, X.W. Wang, et al., Small 19 (2023) 2302652.